Optical Properties of faint FIRST Variable Radio Sources

W. H. de Vries, R. H. Becker
University of California, One Shields Ave, Davis, CA 95616
Lawrence Livermore National Laboratory, L-413, Livermore, CA 94550
devries1@llnl.gov

R. L. White
Space Telescope Science Institute, 3700 San Martin Drive, Baltimore, MD 21218
and

D. J. Helfand
Columbia Astrophysics Laboratory, Columbia University, 550 West 120th Street, New York, NY 10027

ABSTRACT

A sample of 123 radio sources that exhibit significant variations at 1.4 GHz on a seven year base-line has been created using FIRST VLA B-array data from 1995 and 2002 on a strip at $\delta = 0$ near the south Galactic cap. This sample spans the range of radio flux densities from ~ 2 to 1000 mJy. It presents both in size and radio flux density range a unique starting point for variability studies of galaxies and quasars harboring lower luminosity Active Galactic Nuclei (AGN). We find, by comparing our variable and non-variable control samples to the Sloan Digital Sky Survey the following: 1) The quasar fraction of both the variable and non-variable samples declines as a function of declining radio flux density levels; 2) our variable sample contains a consistently higher fraction of quasars than the non-variable control sample, irrespective of radio flux; 3) the variable sources are almost twice as likely to be retrieved from the optical SDSS data than the non-variable ones; 4) based on relative numbers, we estimate that quasars are about five times more likely to harbor a variable radio source than are galaxies; and 5) there does not appear to be any significant optical color offset between the two samples, even though the suggestive trend for sources to be bluer when variable has been detected before and may be real. This leads us to conclude that both radio variability and radio flux density levels, in combination with accurate optical information, are important discriminators in the study of (radio) variability of galaxies. The latter start to dominate the source counts below $\sim$ 20mJy. In any case, variability appears to be an intrinsic property of radio sources, and is not limited to quasars. Radio variability at low flux density levels may offer a unique tool in AGN unification studies.

Subject headings: galaxies: active — galaxies: statistics — quasars: general

1. Introduction

All is flux, nothing stays still; nothing endures but change[1]. This seems to apply particularly well to extragalactic radio sources. Important advances in our understanding of radio source intrinsic and extrinsic variability mechanisms have been made by studying their amplitudes, characteristic time-scales, and cross-correlations with observations at other wavelengths. Radio variability can be classified in three broad classes (Padrielli et al. 1987), based on their frequency depen-

[1]Heraclitus (540-480 BC)

dence: 1) variability only occurs at low frequencies ($\lesssim$ 2GHz), 2) variability occurs both at low and high ($\gtrsim$ 5GHz) frequencies, but is not correlated in time, and 3) low and high frequency variability, but the variations are correlated (although they need not occur simultaneously). This classification also conveniently separates the underlying variability mechanisms into "most likely extrinsic" (low frequency variations only), and "most likely intrinsic" (correlated broadband variability).

The accepted model for the extrinsic variability of radio sources is refractive interstellar scintillation (ISS), which predominantly induces variations at low frequencies ($\lesssim$ 1GHz), with low amplitudes ($\sim$ 2%), and with typical timescales of a few days (Blandford et al. 1986; Rickett 1986). Variations of this type have been detected in multi-frequency studies (e.g., Mitchell et al. 1994; Lazio et al. 2001). Perhaps the strongest arguments for the external origin of these variations are correlations with Galactic latitude (e.g., Gregorini et al. 1986; Gaensler et al. 2000), and an annual modulation due to earth's orbital motion (e.g., Lainela & Valtaoja 1993; Bondi et al. 1994; 1996). Low-frequency variations with much longer timescales ($\sim$ 10 years), and/or larger amplitudes are thought to be source intrinsic, however (e.g., Rýs & Machalski 1990 or, more recently, Gaensler & Hunstead 2000).

Broadband radio variability, in which the variations usually appear first and more strongly at higher frequencies, are thought to be intrinsic to the radio source. A model describing this behavior, in which shocks propagate along the radio jets, has been proposed by Marscher & Gear (1985). The model further implies that sources viewed close to the line of sight (i.e., flat-spectrum quasars and BL Lacs) should be more variable and have shorter variability timescales. For objects very close to the line of sight, relativistic beaming will become important, amplifying the variations and shortening the timescales to $\lesssim$ 1 day (e.g., Lister 2001). Indeed, intraday variability has been readily detected in samples of compact, flat-spectrum sources. Some of the variability occurs on such short timescales that the apparent source brightness temperature (e.g., Gopal-Krishna et al. 1984) can be as high as $T \approx 10^{21}$K (e.g., Quirrenbach et al. 2000), well beyond the inverse Compton limit of 10^{12}K (Kellermann & Pauliny-Toth 1969). Doppler boosting factors of up to a few hundred are needed to reconcile these numbers (the apparent T is proportional to the Doppler factor to the third power). These Doppler factors are actually at the high end of the observed range, and it has been suggested that these velocities are pattern speeds that do not reflect the Lorentz factors of the jet itself (e.g., Lister et al. 2001). Nonetheless, intraday variability has been uniquely identified with the blazar class of objects (e.g., Quirrenbach et al. 1992; Lister et al. 2001).

Comparatively little is known about (intrinsic) radio variability in non-blazar sources at low flux density levels ($\sim$ 10 mJy). Most of the variability research has focused on either bright radio samples (e.g., Gregorini et al. 1986, $S > 0.4$ Jy ; Lister et al. 2001, $S > 0.4$ Jy; Aller et al. 2003, $S > 1.3$ Jy), or small samples at much lower flux levels (a few 10's of mJy – e.g., Rýs & Machalski 1990; Bondi et al. 1996; Riley et al. 1998). Recently, Carilli et al. (2003) used deep multi-epoch VLA[2] observations of the Lockman Hole area to study variability at the 0.1 mJy level, resulting in just 9 variable sources.

In this paper, we will use two epoch observations of the FIRST Zero-Dec strip (Sect. 2) of about 9000 radio sources to expand significantly the number of variable sources down to flux density levels of $\sim$ 1 mJy. Unlike much brighter radio samples, the typical radio source population at these levels is dominated by star-forming galaxies and steep-spectrum systems, with only a small percentage of flat-spectrum AGN (e.g., Windhorst et al. 1999; Richards et al. 1999; de Vries et al. 2002). With our sample, therefore, we are in an excellent position to investigate the radio variability properties of lower radio luminosity galaxies.

Interstellar scintillation is not expected to contribute significantly to the variability in our sources, since our observations were carried out at 1.4 GHz, near the minimum in expected ISS (e.g., Padrielli et al. 1987; Mitchell et al. 1994). Furthermore, given our variability criterion (see Sect. 3), only sources that vary by significant amounts, especially toward the lower flux levels,

[2]The Very Large Array is a facility of the National Radio Astronomy Observatory (NRAO), which is operated by the Associated Universities, Inc., under cooperative agreement with the National Science Foundation.

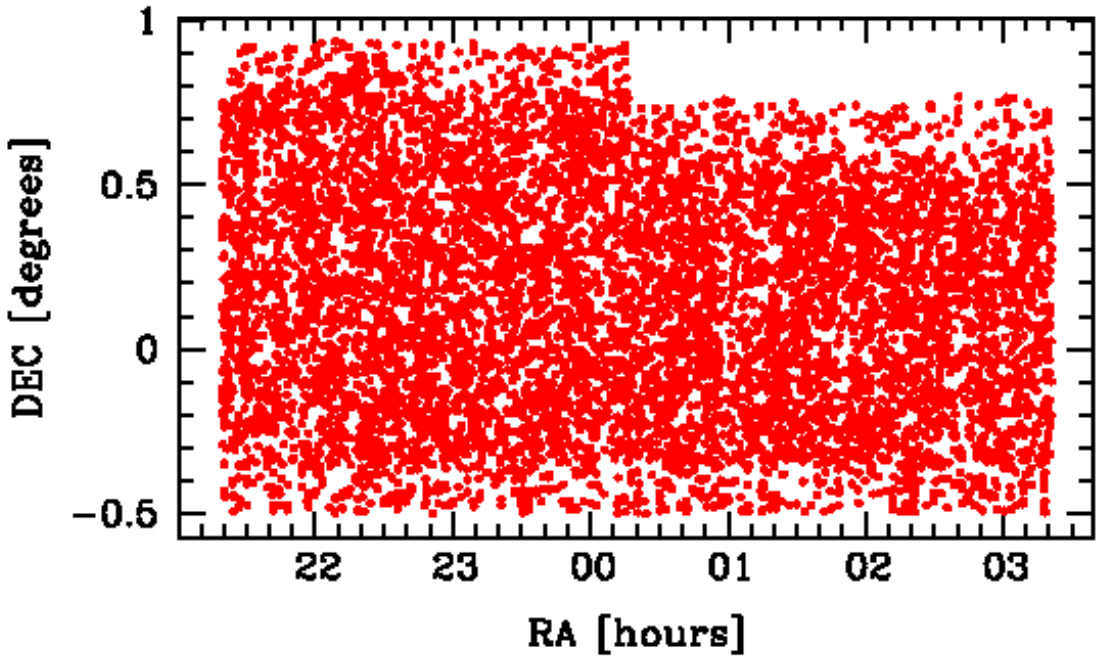

Fig. 1.— FIRST Zero-Dec survey area. Note the non-uniform source density close to the survey boundaries (due to the very different axis scales this is not obvious for the RA edges).

are included. These variation levels exceed the typical ISS variations of a few percent by a large factor.

The paper is outlined as follows. In the next two sections, the radio observations and sample selection are described. In Sect. 5 we discuss the optical properties of the variable sample, and compare these against a non-variable control sample.

2. Observations

Our radio imaging data have been taken as part of the Faint Images of the Radio Sky at Twenty centimeters survey (FIRST, see Becker et al. 1995 for a detailed description) conducted with the VLA in B-array between 1993 and 2002. The observing strategy of the FIRST survey provides a limited capability to search for variability, although since adjacent fields have significant overlap, most sources were observed more than once. For the most part, data were collected in strips of constant declination so adjacent fields in the east-west direction are sensitive to variations on a time scale of 3 minutes. FIRST observing runs were usually separated by multiples of 24 hours so adjacent fields in the north-south direction are sensitive to variations on timescales of 1 to 5 days. This led, for instance, to the discovery of a number of radio-variable stars (Helfand et al. 1999).

A search for variability between the FIRST survey and the NRAO VLA Sky Survey (NVSS, Condon et al. 1998) is also possible. This is, however, complicated by the difference in angular resolution: the FIRST survey can resolve out flux seen by the NVSS. This results in so many NVSS sources appearing brighter than their FIRST counterparts that it is necessary to restrict the analysis to sources which appear brighter in FIRST (see Sect. 3.2), making a straightforward flux comparison to test for variability difficult.

The best opportunity to search for long term variability has been afford by our decision to reobserve the south Galactic cap (SGC) FIRST Zero Dec strip (hereafter FZDB) during the summer of 2002 (the initial set of observation were made in 1995, which will be referred to as FZDA). The observations were made for the dual purpose of a quality control test of the FIRST survey, as well as a search for variability. The zero-dec strip was cho-

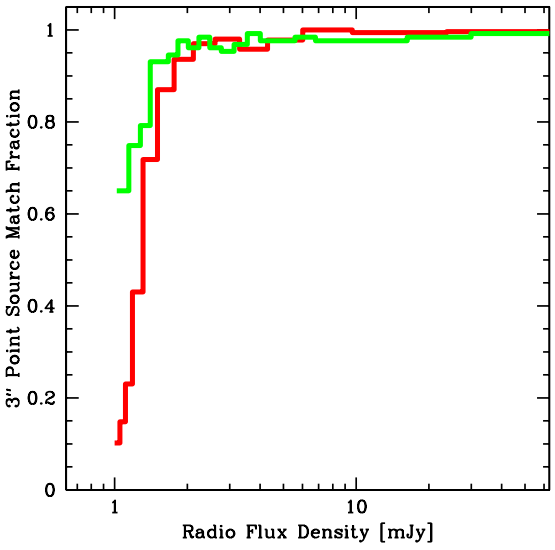

Fig. 2.— Fractions of the FZDA and FZDB catalogs (green and red lines respectively) that are present in the combined catalog. The histograms are for point sources only, and the matching has been done to within 3″. Note the high fractions for sources with flux densities exceeding 2 mJy (98.0% on average). It is also apparent that some fraction of FZDB sources below 2 mJy are spurious, more so than for the FZDA catalog. Each bin represents 500 sources, so the closer spacing toward lower flux density levels reflects the increasing number of faint objects.

sen for this purpose because it has been observed by the Sloan Digital Sky Survey as well (SDSS, see Stoughton et al. 2002 for the Early Data Release, and Abazajian et al. 2003 for Data Release 1 updates). A total of 720 fields were re-observed covering 120.2 square degrees and encompassing 9086 radio objects in the FZDB catalog. The FZDB survey area is shown in Fig. 1.

2.1. Matching FZDB with FIRST

The FIRST catalog has a uniform sensitivity across the surveyed zero-dec strip area, whereas the FZDB has not (Fig. 1). This makes a direct comparison of their relative completeness limits and source surface densities difficult. With an average surface density of ~ 90 radio sources per square degree White et al. (1997), the FIRST catalog should contain about 10 800 objects within the nominal zero-dec strip survey area. However, this number cannot be directly compared to the FZDB count of 9086, due to the latter's non-uniform survey coverage. The best way to compare the two catalogs is to create an FZDA catalog (derived from FIRST) which has its source surface density tapering off toward the survey edges, just like the FZDB catalog. The simplest way of obtaining such a catalog is to list the unique sources contained in FIRST around the FZDB catalog positions. This makes sense, since we are interested in objects present in both catalogs in the first place. The total number of sources in such an FZDA catalog vary with the radius up to which the FZDB positions are matched: 6605 sources within 3″, 7343 within 1′, and 11778 within 10′. We will use the first two lists to compare the relative completeness of the FZDB catalog. The 6605 entry list represents our matched catalog from which we will select our variable sample (Sect. 3.1), and the 7343 constitutes our comparison FZDA sample.

The combined catalog uses a matching radius of 3″, which is about half of the FWHM of the B-array beam. This automatically excludes the fraction of extended sources for which the source detection program assigned different components and/or different positions though. As a consequence, the number of 6605 is considerably lower than the original FIRST surface density (even lower than expected based on the non-uniform coverage). To be consistent, we exclude *all* extended components[3] from our combined sample. There are good scientific reasons for this as well. Extended radio emission is most likely due to lobe (radio hotspot) emission which cannot vary on the short timescales we are sampling here ($7/(1+z)$ years). Since we are interested in shorter timescales, we will have to study those sources in which the (feeding) processes close to the AGN itself vary. These sources are consequently very small, and unresolved by our imaging data (with its resolution of ~ 5 arcseconds). The resulting

[3]We consider a source / component extended if it has a peak flux less than 70% of its integrated flux. It should be noted that we are referring to components, so, for instance, it is possible that a single extended radio source can be resolved into a number of unresolved components, each of which would end up individually in our combined sample; see Sect 4.

reduced sample sizes have been listed in Table 1.

2.1.1. *Sources unique to one catalog - Transient phenomena*

Figure 2 illustrates how well the FZDA and FZDB compare. At the higher flux density levels we expect to find almost all of the point sources in the combined catalog. This is the case for sources with flux densities exceeding 2 mJy. For both the FZDA and FZDB catalogs, over 98% of those sources end up in the combined catalog. None of the remaining catalog-unique entries turned out to be real on close inspection: they were either resolved sources for which a particular component was assigned a differing position between FZDA and FDZB (separated by more than $3''$), or the catalog entry turned out to be an imaging artifact that made it into one but not both catalogs (e.g., ringing around very bright objects).

The situation is quite different for fainter sources, however. An increasing fraction of faint objects are only present in either catalog, which indicates a systematic effect rather than genuine source variability. Disentangling the truly variable sources from the random noise at these flux density levels can only be achieved by obtaining deeper surveys. Indeed, none of these faint sources end up meeting our variability criterion (Sect. 3.1), which is based on the survey sensitivity level. All the variable sources that *do* meet the criterion have flux densities > 2mJy (see Fig. 5), and are in the well-matched part of Fig. 2.

So, in summary, transient phenomena (e.g., Gamma Ray Burst afterglows) have not been found for flux density limits exceeding 2 mJy. Fainter events may be present, but we do not have any way of assessing their reality.

3. Variable sample selection

Since we are interested in radio source variability, we begin by defining our Variability Ratio (hereafter VR) as:

$$\mathrm{VR}(i) = \frac{S(i)_{\mathrm{B}}}{S(i)_{\mathrm{A}}} \qquad (1)$$

for the i^{th} source in our catalog. The indices A and B denote the measurement epochs 1995 and 2002. Because the source brightness does not enter into this equation, we cannot use this ratio at face value: toward the lower flux density levels the (sky background) noise will account for a significant fraction of the "variability" in such sources. We therefore have to weight the VR value of each source individually based on its Signal-to-Noise Ratio (S/N) and local noise values (see next section).

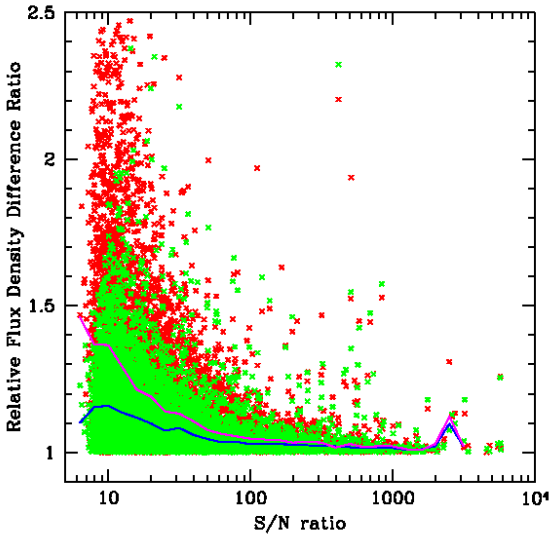

Fig. 3.— Relative flux density ratios for our point source sample as function of S/N. The flux density ratio is defined here as larger flux density divided by smaller flux, irrespective of the epoch (hence it is always > 1). The red points are for the integrated flux density values, and the green points for just the fitted peak values. As can be seen by the overplotted medians (purple for integrated, blue for peak flux densities), the former has a larger scatter, especially toward lower flux density levels.

Since we are only considering unresolved sources, ideally their (fitted) peak flux density and integrated flux density should be the same. This is, however, not the case. In fact, the integrated flux density values are found to have larger intrinsic scatter than the fitted peak flux values. Both the peak and integrated flux density are based on Gaussian fits to the actual data, but unlike the peak fit, the integrated value is also based on fits to the major and minor axes of the object. Noise

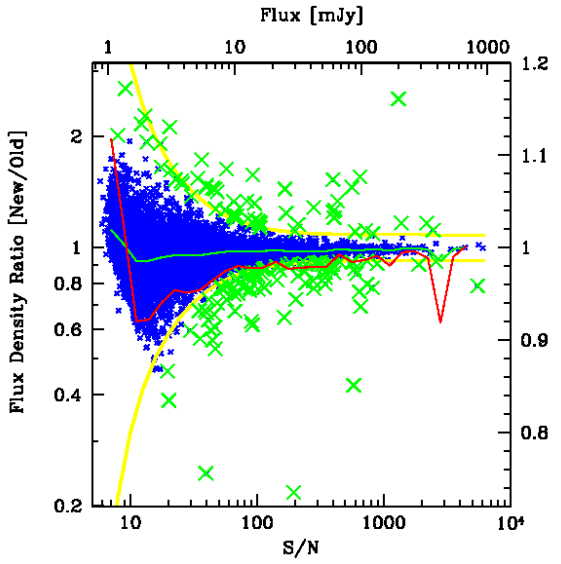

Fig. 4.— Flux density variations for unresolved sources between the two epoch as function of signal-to-noise. The peak flux density value of the most recent epoch has been divided by the 1995 data. The yellow lines represent the 4σ variation limits, as given by Eqn. 4. The highlighted green crosses are sources that meet our variability criterion, the blue crosses are considered non-variable. The solid green line marks the local median variation value, and serves as an indication of the relative calibration between the two epochs. This line has been replotted for better clarity on a linear scale (indicated on the right vertical axis) as a solid red line.

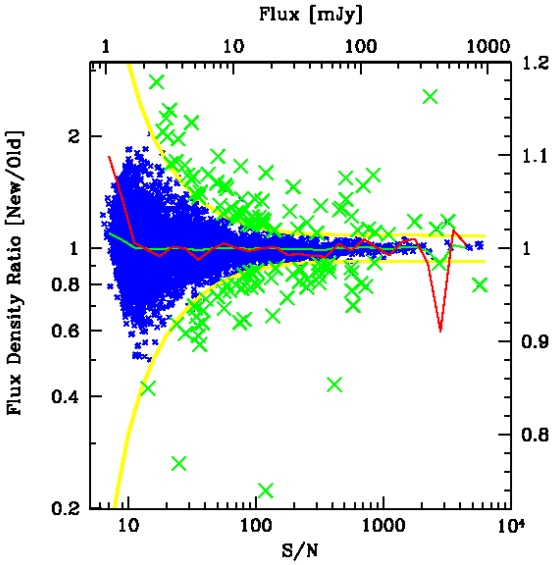

Fig. 5.— The same plot as Fig. 4, but with the adjusted FZDB flux densities: $1.0116 \times (S_B + 0.090$ mJy). This straightens out the median variability curve and evens out the number of positive and negative variable sources.

in the measurement of the axes therefore increases the noise in the integrated flux density compared to the peak value. In Fig. 3 we have plotted the relative flux density difference ratio (defined as the larger flux density divided by the smaller flux density) for both the source integrated and peak flux density values.

It is clear from this figure that the scatter in the peak flux measurements (the solid blue median line) is considerably less than that of the integrated flux density ratios (as indicated by the solid purple median line). To minimize the number of variable false positives, we only consider the source peak flux density values.

3.1. Variability criterion

Following Rengelink et al. (1997), the relative flux density errors can be written as:

$$\frac{\sigma_S}{S} = \left(C_1^2 + C_2^2 \left(\frac{\sigma_{\rm rms}}{S} \right)^2 \right)^{\frac{1}{2}} \qquad (2)$$

This equation reflects the two components of the measurement error, with C_1 due to a constant systematic error, and C_2 dependent on the S/N ratio. This expression can be used to estimate the significance of radio source variation, as defined by the quotient of the new and old flux densities. If one defines the flux density and noise values in the first epoch as S_A,σ_A, and in the second as S_B,σ_B, the 4σ variability envelopes are then given by:

$$\mathrm{VR}_4 = \frac{S_B \left(1 \pm 4\sqrt{C_1^2 + C_2^2 (\frac{\sigma_B}{S_B})^2} \right)}{S_A \left(1 \mp 4\sqrt{C_1^2 + C_2^2 (\frac{\sigma_A}{S_A})^2} \right)} \qquad (3)$$

which can be further reduced by substituting $S_A = S_B = S_{\rm true}$, $\sigma_A = \sigma_B = 0.15$ mJy, $C_1 = 0.01$, and $C_2 = 1.3$. The σ values have been measured to be

on average 0.150 and 0.148 mJy for the 1995 (A) and 2002 (B) epochs, respectively. The C_2 value has been chosen to match the value of Rengelink et al. (1997) and de Vries et al. (2002), and seems fairly robust across different instruments and survey setups. The $C_1 = 0.01$ value (which is lower than the $C_1 = 0.04$ of the latter two papers), is set by the high S/N end of the source distribution. Its adopted value is a good match between including / excluding high S/N variable sources: the fraction of variable sources as function of S/N is kept acceptably flat (see Figs. 4 and 5, with S/N defined as $(S_A + S_B)/(\sigma_A + \sigma_B)$).

The upper and lower 4σ envelopes can now be expressed (as a function of S/N) as:

$$\begin{aligned} \mathrm{VR}_4^{\mathrm{upper}} &= \frac{1+4\chi}{1-4\chi} \\ \mathrm{VR}_4^{\mathrm{lower}} &= \left(\mathrm{VR}_4^{\mathrm{upper}}\right)^{-1} \\ \text{with: } \chi &= \sqrt{0.01^2 + \left(\frac{1.3}{\mathrm{S/N}}\right)^2} \end{aligned} \quad (4)$$

Equation 4 forms the basis of our variability criterion. Any source having a VR exceeding either 4σ envelope is considered genuinely variable. This yields 146 variable sources, of which 58 are brighter in the 2002 epoch, and 88 are fainter (Fig. 4).

The solid red curve in Fig. 4 represents the median flux density ratio as function of S/N, plotted on a linear scale to improve clarity (as opposed to the logarithmic equivalent in green). As can be gathered from this curve, the medians quickly fall below 1 as the S/N decreases, with a maximum deviation of 8% at S/N $\sim$ 10. Most of the offsets are within $\sim$ 2%, however. Even though the offsets are small, there is a systematic trend which is affecting our variability sample selection, something we wish to avoid. If uncorrected, it implies that fainter sources are more likely to fade between 1995 and 2002 than brighter sources, something which would be hard to explain in any variability scenario. We have two parameters to play with: a small (additive) zero-point correction which will straighten out the median curve, and a multiplicative sensitivity correction which will raise or lower the curve along the y-axis. The best correction (with the resulting median curve having the smallest variations along the $\mathrm{VR}_c = 1$ line) is obtained by adjusting the FZDB flux densities by:

$$\mathrm{VR}_c(i) = \frac{1.0116 \times (S(i)_{\mathrm{B}} + 0.090 \text{ mJy})}{S(i)_{\mathrm{A}}} \quad (5)$$

which amounts to a 90 μJy zero-point offset, and a 1.16% sensitivity correction. The 90 μJy offset is small compared to both the 150 μJy rms noise value and the 250 μJy CLEAN bias (a flux density correction applied per beam for the FIRST survey, see White et al. 1997). And the 1.16% factor is well within the nominal $\sim$ 5% systematic uncertainty in the flux density scale.

After applying these corrections (Fig. 5), we end up with 128 candidate variable sources / components (corresponding to 2.0% of the sample), listed in Table 2, of which 70 are brighter in the 2002 epoch, and 58 fainter.

3.2. NVSS comparison

As a reality check, we compared the FZDB catalog against the NVSS catalog to see whether the same sources are deemed variable, using basically an identical variability criterion. There are, however, a few differences. The NVSS survey has a typical background noise of 0.45 mJy (Condon et al. 1998), instead of the 0.15 mJy for the FIRST survey. Another complicating factor is the resolution difference between the NVSS and FZDB. Sources that are not resolved by the 45″ NVSS beam are often resolved by the FZDB, with each component only a fraction of the NVSS total flux density. We tried to minimize this effect by first excluding resolved NVSS sources outright from the correlation, and secondly using the FZDB integrated (instead of peak) flux density measurements. Furthermore, we used a very restrictive 5″ matching radius in another attempt to just match unresolved sources both in the FZDB and NVSS. The resulting matched sample contains 2201 sources.

Of these 2201 sources, 10 are brighter at the FZDB epoch, and 91 are fainter. This is after applying a similar FZDB flux density correction as in the previous section (albeit with slightly different constants). Clearly, there is still some flux density being resolved out by the longer base-line FZDB observations compared to the NVSS, which results in quite a few bogus variable sources.

This implies we cannot really compare the FZDB-NVSS faint variable sources to Table 2, since an unknown fraction of them will be spurious. The 10 FZDB-NVSS bright variable sources on the other hand, are not be affected by this. Indeed, 9 out of the 10 sources are recovered in Table 2 (separately footnoted), with the sole "newly" identified variable source FIRST J222646+005210. Upon closer inspection, this source appears to be stable between FZDA and FZDB (653 ± 1 mJy for both epochs). Its NVSS flux density of 615 mJy is just within the quoted $\sim 5\%$ systematic flux density uncertainty between the two surveys. Based on this, we therefore conclude that our variability criterion is robust, and results in a sample of truly variable sources. This does tacitly assume that the cataloged radio flux densities are always correct. However, as the next section will show, this is actually not valid for some cases.

4. Radio morphology

Our variable sample actually contains 128 variable, unresolved, *components*. While most of these component entries turn out to be single (unresolved) radio pointsources, some of them are part of a multi-component radio source. The varying part is then presumably associated with the AGN / radio-core position. However, there may still be some cases where the FZDA and FZDB cataloging software divided up radio flux differently between adjacent components, introducing artificial variability. It is therefore important to check all the multi-component radio sources in our sample (28) individually.

In order to characterize the *overall* radio properties of our sample, we start by defining 6 morphological categories: 1) Single pointsource (PS in Column 11 of Table 1); 2) Pointsource with an elongation, or linear feature (CJ, "core-jet"); 3) Variable core with two non-variable lobes (CL); 4) Core embedded in diffuse halo (CH); 5) Complex, multi-component structure (CX); and 6) Possible hotspot variability (HS).

Each of the sources in Table 1 have been categorized accordingly. The relative number breakdown of the sample is: 1) 100 (78.1%); 2) 14 (10.9%); 3) 9 (7.0%); 4) 1 (0.8%); 5) 1 (0.8%); and 6) 3 (2.3%). Except for the last two classes (containing 4 sources, or 3.1% of the total sample), all of the variability is consistent with it being due to the AGN / core component. We will discuss a few selected sources in more detail below. Radio maps of all the extended variable radio sources can be found in Fig. 10.

J000257−002447 (CH) – This source contains a variable pointsource component embedded in an extended radio halo. The radio surface brightness of this halo remains constant between the FZDA and FZDB epochs, whereas the peak flux density of the central pointsource varies by more than 10%.

J001800+000313 (HS) – The North-Eastern lobe of this double radio source is slightly resolved, just enough so that it did not make it into our variable component list. As it turns out, both lobes / hotspots appear to be variable. The total flux density for the radio source increased by 13.6% between FZDA and FZDB, from 62.14 to 70.56 mJy. Unfortunately, two unrelated sources close to this source also "varied" by $\sim 10\%$, casting serious doubt on its reality. The source is very close to the edge of its particular survey field, which may be the reason for the flux density discrepancy. It is taken out of further consideration, and has been placed separately in Table 1.

J003246−001917 (HS) – Upon close inspection of both the FZDA and FZDB catalogs, we have to come to the conclusion that this source is not variable. The problems stems from the fact that FZDA lists 5 components for this source, and FZDB only 4. This leads to quite different flux density assignments to the North-Western lobe. The source is taken out of further consideration.

J012213−001801 (CL) – Both the Eastern and Western lobes are constant to within $\sim 1\%$ between FZDA and FZDB. Flux density values for the bright Eastern lobe are 123.84 and 122.61 mJy, a variation of 1.0%. The core, on the other hand, brightened over the same time period from 348.28 to 404.79 mJy.

J020234+000301 (CL) – The lobes do not vary beyond the 1% level. The core, however, fades from its FZDA flux of 44.01 mJy to 35.92 (an 18.4% decrease).

J021840−001515 (CX) – This is the only source in our sample with a hard to categorize radio morphology. The marked component position (Fig. 10) coincides with a $z = 1.171$ quasar. The

two components immediately to the North do not have optical counterparts, though there appears to be a faint object in the SDSS image that is situated in between the lobes. All of the radio components fade between FZDA and FZDB by on average 16%. A nearby, unrelated, radio source observed in the same field remains constant, however. The component associated with the quasar varies the most: from 14.12 mJy down to 10.92 mJy (a decline of 22.7%). At the moment it is not clear to us how the various components relate to each other, if at all.

J021202−002750 (CL) – The core component faded by at least 4 mJy ($\sim$ 8%) relative to the lobes.

J212058+000612 (HS) – As is the case for J003246−001917, this source is not variable. The South-Eastern lobe is constant, and the perceived variability in the North-Western lobe is due to differing FZDA and FZDB component flux density assignments. This source is also taken out of consideration.

J212955+000758 (CL) – The "variability" is due to the FZDA having 3 components, whereas FZDB lists 4. The summed fluxes do not vary.

J220017−000133 (CL) – The core component in this source brightened (by 20%), so we are inclined to regard this source as variable even though the number of fitted components is different between the FZDA and FZDB. This faint extra component in the FZDA catalog (just to the North of the core) does not appear to contribute anything to the total flux of the core in the FZDB catalog (where this component is absent), based on the fitting parameters.

J222729+000522 (CL) – The core variability is 17.2% (relative to the lobes), with the flux declining from 97.51 mJy to 80.69 mJy.

J235050−002848 (CL – The core flux increased, whereas the lobes remained more or less constant.

J235828+003934 (CL – All of the components faded by about the same amount, casting serious doubt on the reality of core variability. We have taken this source out of further consideration.

So, after close inspection, we found all 3 potential hotspot variable sources (HS) and 2 core-lobe (CL) sources to be non-variable. They have been excluded from our subsequent studies, but are left in Table 1 and Fig. 10 as reminders of how careful one has to be using automated selection criteria.

5. Optical identifications - Detection rates

We next investigate the possible connection between optical properties and the presence of radio variability. Variability correlations in the optical and radio have been proposed before (e.g., Tornikoski et al. 1994; Hanski et al. 2002), with the highly beamed blazars as the clearest examples of sources which exhibit variability across the electromagnetic spectrum (e.g., Bregman et al. 1990). The first step would be to correlate our variable sample with known optical catalogs, and compare the results against a sample of non-variable radio sources. We therefore created 12 sets of 123 non-variable sources (i.e., each control sample has the same number of elements as the variable sample). To ensure non-variability, we only selected sources inside 1σ variation curves (as opposed to sources *outside* 4σ variations, Fig. 5), while matching the radio flux density distribution function of the variable sample. This was done by matching the number of non-variable sources to the amount of variable sources per S/N bin (binned logarithmically from 1.0 to 3.4, with binsize 0.4 dex). Given that there are only 1922 sources (out of our initial sample of 6605) that are less variable than these 1σ limits, 12 sets of control samples are about as many as one can create without starting to have a significant fraction of sources shared between them.

All of our FZDA/FZDB survey area is covered by the Automatic Plate Measuring (APM) machine catalog. The APM facility (in Cambridge, UK) lists identifications and positions based on scanned UK and POSS II Schmidt plates, covering currently more than 15, 000 deg^2 of sky.

5.1. APM matches

Our sample of 123 variable sources has been matched against the APM catalogs with a $3''$ matching radius. While this does discriminate against possible off-nuclear radio sources, it is necessary to limit the number of chance matches, given the density of objects in the APM catalog. The matching results are listed in Table 3. What is immediately striking is the difference in detection rates between the variable and non-variable samples. About half of the variable sources are

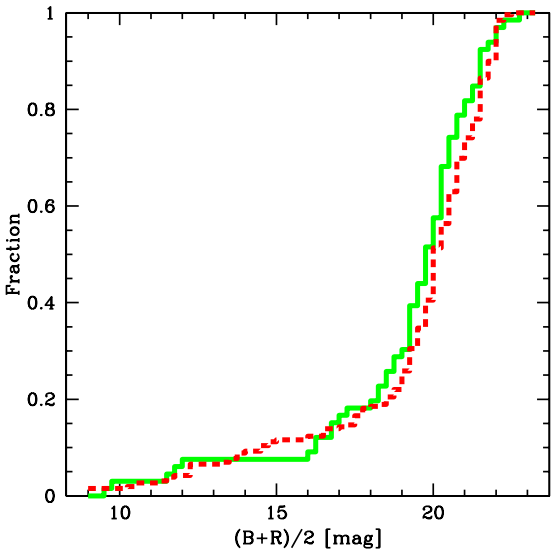

Fig. 6.— Cumulative magnitude distribution of radio sources which are identified by the APM (66 variable sources in total). The solid green line is for our variable sample, the dashed red line represents the distribution for the combined 12 non-variable (less than 1σ) control samples (262 sources in total). Both distributions are identical, based on a KS-test (using 0.25 magnitude bins, for a total of 56).

retrieved from the APM catalogs, but only 1 in 6 of the non-variable sources have optical counterparts. The rms variation between the 12 control samples is 2.8%, resulting in a $\sim 13\sigma$ detection rate difference. Clearly, variable sources are easier to detect not only because on average they are brighter, but also due to a higher fraction of quasars[4] (see Sect. 5.2). The brightness difference is not large; actually a cumulative distribution plot against mean magnitude (Fig. 6) shows how comparable their distributions are. Based on a KS-test, these two distributions do not differ to any level of significance.

Fortunately, a significant fraction ($\sim$ 60%) of the survey is covered by the SDSS Data Release 1 (DR1), so we can use these deeper and more uniform imaging data to investigate this further.

[4]without spectroscopic confirmation, most of these objects should be considered quasar candidates.

5.2. SDSS

The SDSS data also show a higher fraction of optical identifications for variable sources. Since the latter data are deeper than the photographic plates the APM catalogs are based on, we identify 82% of the variable sources, and on average 38% of the non-variable ones (Table 4). These values are up from the APM values of 54% and 18%, respectively. As mentioned earlier, one way of explaining the higher match rate for the variable sample is that it may contain a higher fraction of quasars. Since these objects are typically unresolved, they are easier to detect at any given magnitude than resolved galaxies (of the same integrated magnitude). Table 4 lists the morphological breakdown of each sample, based on the SDSS classification. With a relative stellar fraction of 53%, the variable sample contains significantly more quasar candidates than the non-variable control sample (on average 19%).

The results of Table 4 can also be used to calculate how much more quasars are likely to be variable compared to galaxies. This is a function of radio flux density (Fig. 7), but the low number of sources (per bin) only allow for an overall ratio. We assume the non-variable sample numbers (19% of the radio population are quasars, 81% are galaxies) are representative of the general population. These numbers compare very well to the ones quoted by Ivezić et al. (2002) for a much larger sample of SDSS sources detected with FIRST (83% of those are galaxies). Now, if we introduce the terms quasar variability rate QVR and galaxy variability rate GVR (both defined as the fraction of quasars / galaxies that are variable), and an initial sample size of P, we get:

$$\begin{aligned} 0.19 \times P \times \mathrm{QVR} &\equiv \#\text{ of quasars in var. sample} \\ 0.81 \times P \times \mathrm{GVR} &\equiv \#\text{ of galaxies in var. sample} \end{aligned} \quad (6)$$

This means that the variable sample will contain in total $(0.19 \times P \times \mathrm{QVR} + 0.81 \times P \times \mathrm{GVR})$ variable sources. We know the relative quasar and galaxy fractions to be 53% and 47%. This leads to (after dividing out P):

$$0.19 \times \mathrm{QVR} = 0.53 \times (0.19 \times \mathrm{QVR} + 0.81 \times \mathrm{GVR}) \Leftrightarrow$$

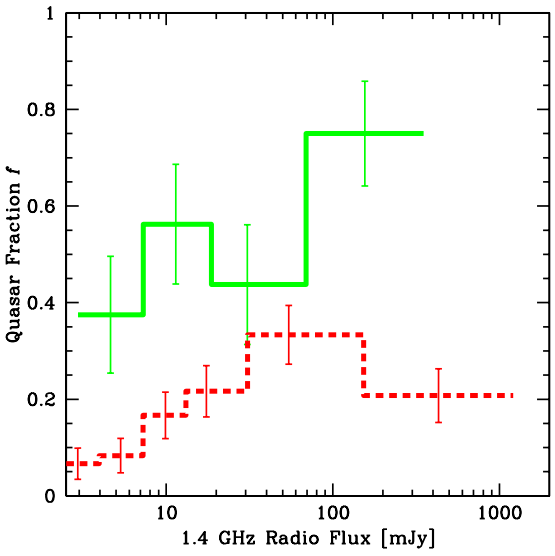

Fig. 7.— Quasar population fraction as a function of radio flux density. The solid green line denotes the quasar fraction for our sample (64 objects in total, 16 per bin), and the dashed red line indicates the fraction for our non-variable control sample (341 sources in total, 60 per bin). The error-bars are given by the formal binomial distribution error: $\sigma(f) = (f(1-f)/N)^{0.5}$.

$$\mathrm{QVR} = \frac{0.53 \times 0.81}{0.47 \times 0.19}\ \mathrm{GVR} = 4.8\ \mathrm{GVR} \qquad (7)$$

If one assumes a $\sim$ 6% uncertainty in the relative fractions (Table 4), this relative value ranges between 3.4 and 7.5. In other words, not surprisingly, quasars are on average 5 times as variable (in the radio) than are galaxies.

5.3. Classification as function of radio flux density

The radio source population changes as a function of radio flux density (e.g., Windhorst et al. 1999; Richards et al. 1999; de Vries et al. 2002), from mainly AGN-dominated sources at higher flux density levels down to starburst dominated sources at the sub-mJy level. This will affect our variable sample as well, and we expect to see a decline of the quasar fraction as function of lower flux density limits. This is nicely illustrated in Fig. 7, which plots the relative quasar fraction with flux density. The solid green line represents our variable sample, and the dashed red line is the mean of our 12 control samples. The bins have a constant number of members (except for the last bin in the control sample), hence the variable spacing. The binning of the control samples has been adjusted to approximately match the binning of the actual sample (4 bins of 16 each for the variable sample, and 5 bins of 60 plus 1 bin of 41 members for the control samples).

While it is not known how much uncertainty is present in the SDSS classification (and hence quasar fraction) toward the faintest magnitudes (see Sect. 5.3.1 below), it is apparent from Fig. 7 that the quasar fractions for the variable and non-variable samples differ significantly (the formal fraction errors are 5% for the control sample, and 12% for the variable sample). This leads us to two robust conclusions based on this figure: 1) a radio variable sample will contain more quasars than a non-variable sample, irrespective of radio flux density, and 2) the relative contribution of quasars to the sample declines as a function of declining flux density: below $\sim$ 20mJy, galaxies account for the majority of the variable sources.

5.3.1. Classification reliability

The last section critically hinges on the reliability of the SDSS galaxy versus quasar classification scheme. If for one reason, most of the excess quasar classifications in our variable sample were made toward the very faint end of the magnitude range, one might become suspicious about the reality of the effect. A direct test is plotting the quasar fraction as function of optical (R-band in this case) magnitude, instead of radio flux density as in Fig. 7. This has been done in Fig. 8, with again our variable sample in green and the control sample in red. It is reassuring to see that most of the excess quasar identifications in the variable sample are made for magnitudes brighter than $R \sim 21$. Stoughton et al. (2002) estimate a 95% confidence level for classifications up to this magnitude. It becomes much less certain for fainter sources. Without doubt some of the current classifications are wrong, but there is no indication that our consistently higher quasar fraction in the variable sample, both as function of radio flux density and optical magnitude, is significantly affected by this.

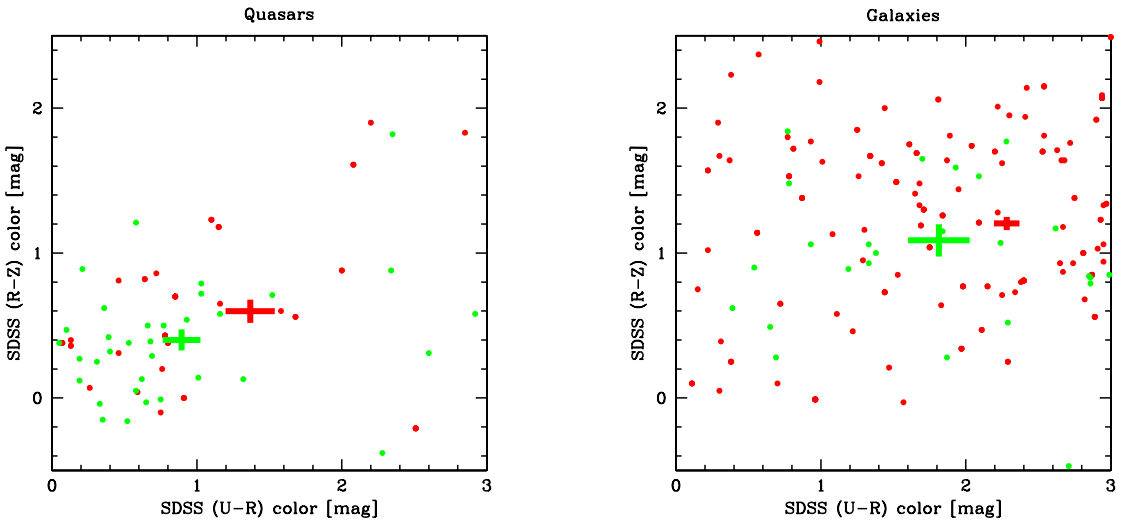

Fig. 9.— SDSS (r−z) versus (u−r) color plots. The variable sample is represented in green, with quasars and galaxies in the left and right panels respectively. The control sample is presented in red. The crosses mark the sample *mean* colors and their 1σ errors along each axis (values are given in Table 5). The optical color offset between the variable and non-variable samples are significant at the $\sim 2\sigma$ level. This trend for variable sources to become bluer during an outburst has been seen before (e.g., Trevese & Vagnetti 2002). Note also that the the quasars are generally bluer (i.e., lower u−r and r−z colors) than the galaxies.

5.4. Optical colors

We have established that there is a significant difference between the variable and non-variable radio samples in terms of their optical counterparts. The former have a higher matching rate with optical identifications (given a fixed detection limit), which is at least in part ascribed to the higher fraction of quasars. We have already seen that the magnitude distributions are not significantly different (Fig. 6), however, this does not rule out that significant optical color differences may be present between the samples. The clearest difference between galaxies and quasars (at least in the restframe) is provided by the (u−r) vs (r−z) color plot (see Fig 13 in Stoughton et al. 2002 for intermediate color-color plots). This allows for sampling of the 4000Å break in galaxies up to a redshift of about unity. This break will offset the galaxies from the quasars, which usually exhibit fairly flat, powerlaw continua (see Fig. 3 in de Vries et al. 2003). Our data are presented in Fig. 9. The sample means and their 1σ errors (indicated by the crosses in Fig. 9) are presented in Table 5. Both the variable quasar and galaxy distributions in the color-color plane are (statistically) distinct from the non-variable control sample. This trend for both the galaxies and quasars to become bluer when they vary has been seen before (e.g., Giveon et al. 1999; Trevese & Vagnetti 2002; Vagnetti et al. 2003; de Vries et al. 2003). Still, the color spread among the sources in the sample is much larger than the *individual* color change as a source goes through an outburst. Indeed, the studies of Giveon, Trevese, Vagnetti and their respective collaborators all rely on following individual objects through their outbursts, instead of using a statistical sample.

The presence of the mean optical color offsets in our radio variable sample implies two things: 1) on average, radio variable sources also exhibit optical (color) variations, and 2) the optical variation time-scales are shorter than our 7 year baseline, since the SDSS data were not taken at the epoch of radio outburst. However, optical colors for an individual source, while useful in differentiating between quasars and galaxies, do not provide an effective selection mechanism for (radio) variability. Nonetheless, as we have seen in the previous sections, the presence of radio variability has a clear impact on the sample's morphological

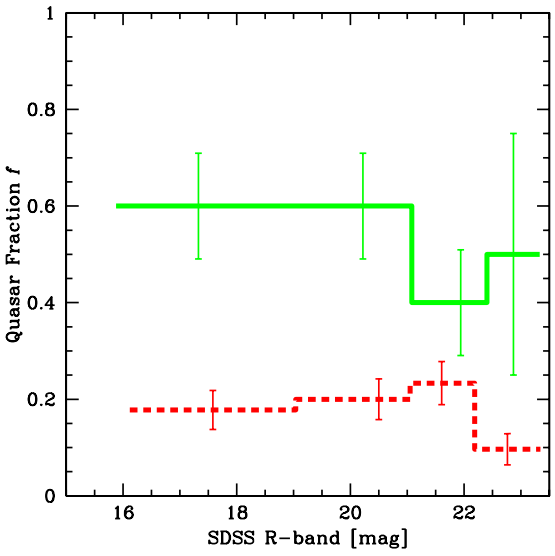

Fig. 8.— Quasar population fraction as function of R-band magnitude. Like in Fig. 7, the solid green line denotes the quasar fraction for our variable sample, and the dashed red line is for the non-variable control sample. We applied slightly larger bins here (20 and 90 objects for the variable and control samples). Note that most of the excess quasars in the variable sample are toward the brighter magnitudes (R<21), and can be considered reliably classified. Error-bars as defined in Fig. 7.

makeup.

6. Summary

We have created a sample of 123 variable radio sources using two epoch observations of a zero-dec strip toward the south Galactic cap. This sample spans the range of radio flux densities from ~ 2 to 1000 mJy. It presents both in size and radio flux density coverage a unique starting point for variability studies of more normal, less AGN-dominated galaxies, especially toward the lower flux density limits. We compared both our variable and non-variable samples to the Sloan Digital Sky Survey optical data.

We found that the quasar fraction of the sample sharply declines as a function of declining radio flux density levels. This is consistent with earlier findings that the radio source population demographics change as one samples at progressively lower flux density levels: AGN-dominated systems tend to be found at the brighter radio flux density levels (> 10 mJy), whereas star-forming and normal galaxies dominate the counts at sub-mJy flux density levels (at 1.4 GHz, e.g., Windhorst 2003). Our variable sample contains a consistently higher fraction of quasars than the non-variable control sample, independent of radio flux density. While this explains part of our almost $2\times$ higher optical matching rate of the variable sample compared to the non-variable one (quasars are easier to detect at a given brightness limit than galaxies), it does imply that our variable sample contains on average slightly brighter sources (though not significantly so, see Sect. 5.1). Based on relative number statistics, we estimate that quasars are about 5 times more likely to harbor a variable radio source than galaxies. However, at flux density levels < 20 mJy, the majority of (radio) variable sources are identified as galaxies. And finally, galaxies and quasars that harbor a variable radio source exhibit, on average, bluer optical colors than hosts of non-variable sources.

All of this underlines the fact that both galaxies and quasars can harbor variable radio sources, albeit at different occurrence rates. Some of this is obviously due to the beamed nature of the (variable) quasars, enhancing the variability both by boosting their brightnesses and shortening the variability timescales[5]. Nonetheless, especially toward lower radio flux density limits, a statistically significant study of variability is possible provided one starts with large enough samples. Large scale optical surveys like the SDSS provide the crucial radio source optical "environmental" information. As more SDSS data become available on the zero-dec strip, we will investigate this further.

The authors like to thank Steve Croft for useful discussions and careful reading of this paper. WDVs work was performed under the auspices of the U.S. Department of Energy, National Nuclear Security Administration by the University of California, Lawrence Livermore National Laboratory under contract No. W-7405-Eng-48. The authors also acknowledge support from the National

[5]Even though blazars represent a very small fraction of AGN, they are much more common in variable samples.

Radio Astronomy Observatory, the National Science Foundations (grants AST 00-98259 and AST 00-98355), the Space Telescope Science Institute, and Microsoft. This research has made use of the NASA/IPAC extragalactic database (NED) which is operated by the Jet Propulsion Laboratory, Caltech, under contract with the National Aeronautics and Space Administration.

REFERENCES

Abazajian, K., et al. 2003, AJ, 126, 2081

Aller, M. F., Aller, H. D., & Hughes, P. A. 2003, ApJ, 586, 33

Becker, R. H., White, R. L., & Helfand, D. J. 1995, ApJ, 450, 559

Blandford, R., Narayan, R., & Romani, R. W. 1986, ApJ, 301, L53

Bondi, M., Padrielli, L., Gregorini, L., Mantovani, F., Shapirovskaya, N., & Spangler, S. R. 1994, A&A, 287, 390

Bondi, M., Padrielli, L., Fanti, R., Ficarra, A., Gregorini, L., & Mantovani, F. 1996, A&AS, 120, 89

Carilli, C. L., Ivison, R. J., & Frail, D. A. 2003, ApJ, 590, 192

Condon, J. J., Cotton, W. D., Greisen, E. W., Yin, Q. F., Perley, R. A., Taylor, G. B., & Broderick, J. J. 1998, AJ, 115, 1693

de Vries, W. H., Morganti, R., Röttgering, H. J. A., Vermeulen, R., van Breugel, W., Rengelink, R., & Jarvis, M. J. 2002, AJ, 123, 1784

de Vries, W. H., Becker, R. H., & White, R. L. 2003, AJ, 126, 1217

Gaensler, B. M., & Hunstead, R. W. 2000, PASA, 17, 72

Giveon, U, Maoz, D., Kaspi, S., Netzer, H., & Smith, P. S. 1999, MNRAS, 306, 637

Gregorini, L., Ficarra, A., & Padrielli, L. 1986, A&A, 168, 25

Hanski, M. T., Takalo, L. O., & Valtaoja, E. 2002, A&A, 394, 17

Helfand, D. J., Schnee, S., Becker, R. H., White, R. L., & McMahon, R. G. 1999, AJ, 117, 1568

Ivezić, Z., Menou, K., Knapp, G. R., et al., 2002, AJ, 124, 2364

Kellermann, K. I., & Pauliny-Toth, I. I. K. 1969, ApJ, 155, L71

Lainela, M., & Valtaoja, E. 1993, ApJ, 416, 485

Lazio, T. J. W., Waltman, E. B., Ghigo, F. D., Fiedler, R. L., Foster, R. S., & Johnston, K. J. 2001, ApJS, 136, 265

Lister, M. L. 2001, ApJ, 561, 676

Lister, M. L., Tingay, S. J., & Preston, R. A. 2001, ApJ, 554, 964

Magdziarz, P. 1995, A&A, 299, 650

Marscher, A. P., & Gear, W. K. 1985, ApJ, 298, 114

Minns, A. R., & Riley, J. M. 2000, MNRAS, 315, 839

Mitchell, K. J., Dennison, B., Condon, J. J., Altschuler, D. R., Payne, H. E., O'Dell, S. L., & Broderick, J. J. 1994, ApJS, 93, 441

Padrielli, L, Aller, M. F., Aller, H. D., et al. 1987, A&AS, 67, 63

Paredes, J. M., Marti, J., Jordi, C., Trullols, E., & Peracaula, M. 1993, A&AS, 102, 381

Peng, B., Kraus, A., Krichbaum, T. P., & Witzel, A. 2000, A&AS, 145, 1

Quirrenbach, A., Witzel, A., Krichbaum, T. P., Hummel, C. A., Wegner, R., Schalinski, C. J., Ott, M., Alberdi, A., & Rioja, M. 1992, A&A, 258, 279

Quirrenbach, A., Kraus, A., Witzel, A., Zensus, J. A., Peng, B., Risse, M., Krichbaum, T. P., Wegner, R., & Naundorf, C. E. 2000, A&AS, 141, 221

Rengelink, R. B., Tang, Y., de Bruyn, A. G., Miley, G. K., Bremer, M. N., Röttgering, H. J. A., & Bremer, M. A. R. 1997, A&AS, 124, 259

Richards, E. A., Fomalont, E. B., Kellermann, K. I., Windhorst, R. A., Partridge, R. B., Cowie, L. L., & Barger, A. J. 1999, ApJ, 526, L73

Rickett, B. J. 1986, ApJ, 307, 564

Riley, J. M., & Green, D. A. 1998, MNRAS, 301, 203

Romero, G. E., Benaglia, P., & Combi, J. A. 1997, A&AS, 124, 307

Rys, S, & Machalski, J. 1990, A&A, 236, 15

Stoughton, C., Lupton, R., et al. 2002, AJ, 123, 485

Tornikoski, M., Valtaoja, E., Teräsranta, H., Smith, A. G., Nair, A. D., Clements, S. D., & Leacock, R. J. 1994, A&A, 289, 673

Trevese, D., & Vagnetti, F. 2002, ApJ, 564, 624

Vagnetti, F., Trevese, D., & Nesci, R. 2003, ApJ, 2003, 590, 123

White, R. L., Becker, R. H., Helfand, D. J., & Gregg, M. D. 1997, ApJ, 475, 479

Windhorst, R. A., Hopkins, A., Richards, E. A., & Waddington, I. 1999, in "The Hy Redshift Universe", ASP Conference Series, Vol 193, eds. A. J. Bunker & W. J. M. van Breugel, p. 55

Windhorst, R. A. 2003, New Astronomy Reviews, 47, 357

This 2-column preprint was prepared with the AAS LaTeX macros v5.2.

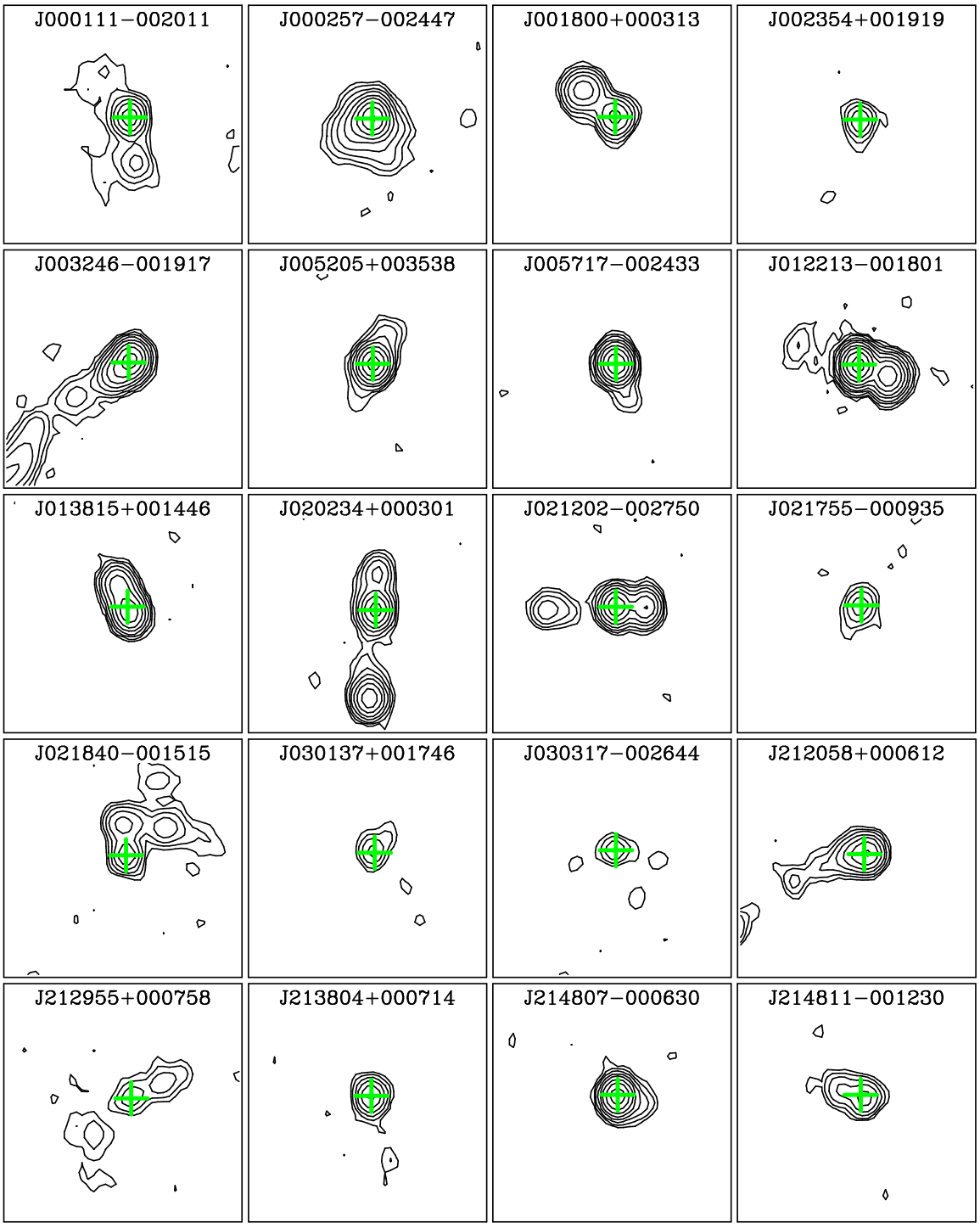

Fig. 10.— FZDA images of the extended subset of our variable sample (28 sources in total). The boxes are $72'' \times 72''$ in size. The variable component is indicated by the green cross.

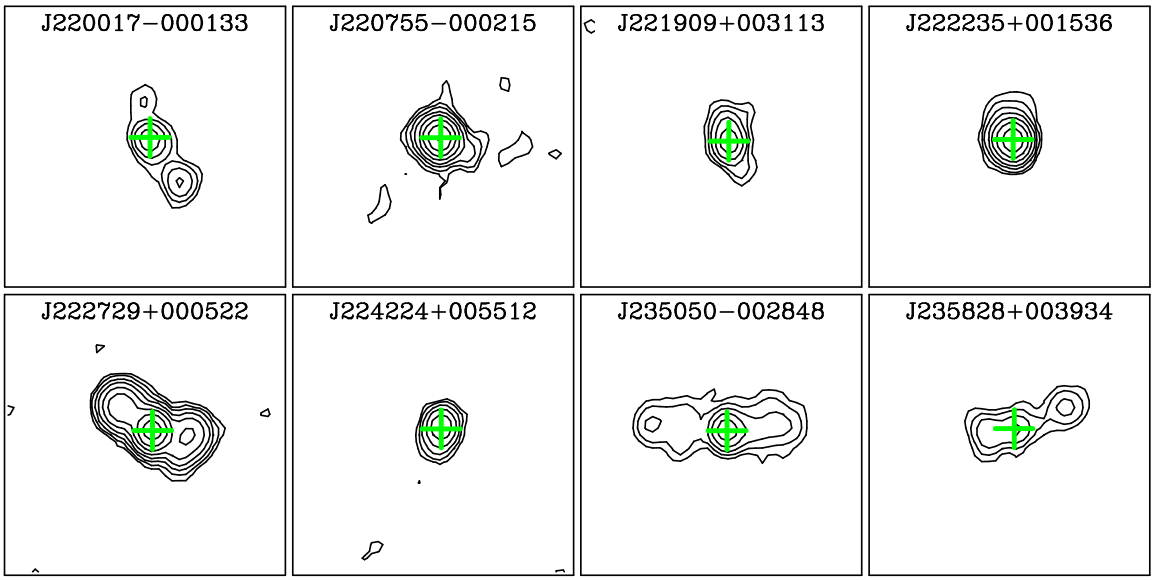

Fig. 10.— continued

TABLE 1
FZDA / FZDB SAMPLE STATISTICS

Sample	Total Number	Point Sources Only
FZDA	7343	5550
FZDB	9086	7286
Combined	6605	5172
FZDB not in A	2481	1846

TABLE 2
FIRST ZERO-DEC VARIABLE SAMPLE

Source / Component	RA (J2000) (core component)	Dec (J2000) (core component)	F_{2002} [mJy]	F_{1995} [mJy]	FR[a]	S[b]	z[c]	r[c]	ID[c]	RM[d]
J000111−002011	00 01 11.19	−00 20 11.6	33.57	23.28	1.46	15.6	0.518	18.56	Q	CL
J000257−002447	00 02 57.19	−00 24 47.4	112.93	124.90	0.92	4.2		19.52	G	CH
J000549+005048	00 05 49.92	00 50 48.1	8.87	5.13	1.77	10.1		21.59	G	PS
J001158−000208	00 11 58.81	−00 02 08.2	5.95	27.34	0.22	43.2		20.98	Q	PS
J001507−000801	00 15 07.01	−00 08 01.8	10.54	12.67	0.85	4.3	1.704	18.23	Q	PS
J001611−001512	00 16 11.07	−00 15 12.3	827.61	1050.26	0.80	11.2	1.575[e]	19.70	Q	PS
J002354+001919	00 23 54.58	00 19 19.5	4.75	7.46	0.66	5.2		22.69	G	CJ
J002738+000627	00 27 38.25	00 06 27.6	4.56	6.91	0.68	5.4		22.02	Q	PS
J003007−000007	00 30 07.90	−00 00 07.4	50.52	39.32	1.30	12.1		19.55	Q	PS
J003127+003959	00 31 27.92	00 39 59.4	9.58	12.31	0.79	6.3		21.80	Q	PS
J003536−000627	00 35 36.30	−00 06 27.2	17.28	14.52	1.21	6.1		18.94	G	PS
J003540−002529	00 35 40.22	−00 25 29.2	4.01	6.57	0.63	6.4		21.82	G	PS
J003703+003537	00 37 03.36	00 35 37.4	12.84	15.28	0.86	4.5		21.51	Q	PS
J004332+002459	00 43 32.71	00 24 59.8	120.94	108.53	1.13	6.1	1.127[e]	19.20	Q	PS
J004819+001457	00 48 19.11	00 14 57.1	98.76	89.40	1.12	5.6	1.536[e]	19.92	Q	PS
J005205+003538	00 52 05.58	00 35 38.2	34.58	81.46	0.43	38.1	0.399	16.09	Q	CJ
J005212+000945	00 52 12.47	00 09 45.2	11.92	9.77	1.24	5.5				PS
J005225+002627	00 52 25.67	00 26 28.0	12.13	9.98	1.24	5.2		20.75	G	PS
J005717−002433	00 57 17.01	−00 24 33.2	89.47	114.74	0.79	11.6	2.790[e]	19.19	Q	CJ
J010525+001121	01 05 25.52	00 11 21.7	33.97	41.73	0.83	8.3		21.45	G	PS
J010745+003952	01 07 45.21	00 39 52.8	10.50	8.88	1.21	4.5				PS
J010838+002814	01 08 38.56	00 28 14.6	5.33	3.91	1.40	4.2				PS
J011106+000846	01 11 06.79	00 08 46.1	5.25	3.43	1.57	4.9		22.70	Q	PS
J011515+001248	01 15 15.78	00 12 48.5	46.84	43.13	1.10	4.4	0.045	14.39	G	PS
J012213−001801	01 22 13.92	−00 18 01.0	386.60	331.60	1.18	8.3		20.23	Q	CL
J012528−000555	01 25 28.85	−00 05 55.8	1333.76	1481.35	0.91	4.8	1.076	16.47	Q	PS
J012753+002516[f]	01 27 53.70	00 25 16.5	131.32	90.08	1.48	19.1		20.76	Q	PS
J013457+003942	01 34 57.42	00 39 43.0	6.09	2.87	2.18	8.7		22.04	Q	PS
J013815+001446	01 38 15.02	00 14 46.5	42.98	51.76	0.84	8.1		21.64	G	CJ
J015329−002214	01 53 29.75	−00 22 14.3	17.46	14.98	1.19	5.8		19.07	Q	PS
J015528+001204	01 55 28.47	00 12 04.6	17.23	19.82	0.88	4.8		22.08	G	PS
J015950−002407	01 59 50.09	−00 24 07.2	10.68	12.63	0.86	4.3		21.50	G	PS
J020141+003825	02 01 41.04	00 38 25.5	4.50	6.35	0.73	4.7				PS
J020214−001748	02 02 14.30	−00 17 48.3	75.12	60.00	1.27	11.5		21.36	G	PS
J020234+000301	02 02 34.32	00 03 01.7	30.54	39.41	0.79	10.5		18.42	G	CL
J020928−001224	02 09 28.85	−00 12 24.9	4.10	2.51	1.69	4.2	0.152	16.02	G	PS
J021202−002750	02 12 02.13	−00 27 50.1	45.14	52.84	0.87	6.6				CL
J021301−001815	02 13 01.13	−00 18 15.0	41.55	48.44	0.87	6.5		21.98	G	PS
J021553+001826	02 15 53.65	00 18 26.9	30.90	35.82	0.88	5.6		19.51	G	PS
J021755−000935	02 17 55.99	−00 09 35.9	3.96	5.85	0.70	4.4		19.86	G	CJ
J021840−001515	02 18 40.55	−00 15 15.9	10.06	13.17	0.78	6.4	1.171	18.81	Q	CX
J022624+000746	02 26 24.61	00 07 46.2	43.84	48.74	0.91	4.4		22.56	G	PS
J023105+000843	02 31 05.59	00 08 43.5	47.60	53.86	0.90	5.0	1.338	20.00	Q	PS
J025321+000559	02 53 21.04	00 05 59.9	151.89	97.64	1.57	22.0		22.26	G	PS

TABLE 2—*Continued*

Source / Component	RA (J2000) (core component)	Dec (J2000) (core component)	F_{2002} [mJy]	F_{1995} [mJy]	FR[a]	S[b]	z[c]	r[c]	ID[c]	RM[d]
J025333+002431	02 53 33.66	00 24 31.7	16.86	14.86	1.15	4.6				PS
J025404−002628	02 54 04.60	−00 26 28.7	4.39	2.71	1.67	5.2		21.97	G	PS
J025859+003618	02 58 59.65	00 36 18.3	29.45	23.75	1.26	9.4		22.28	Q	PS
J025928−002000[f]	02 59 28.52	−00 20 00.1	243.47	225.85	1.09	4.3	2.001	17.34	Q	PS
J030137+001746	03 01 37.58	00 17 46.1	6.86	4.45	1.58	7.0		21.47	G	CJ
J030317−002644	03 03 17.01	−00 26 45.0	7.41	3.68	2.06	4.9				CJ
J030702+000651	03 07 02.04	00 06 51.9	5.84	8.08	0.74	5.4				PS
J030834+003303	03 08 34.31	00 33 03.7	4.16	1.83	2.35	6.4	0.031	14.91	G	PS
J030933−001901	03 09 33.27	−00 19 01.2	6.31	4.58	1.41	4.6				PS
J031006+001549	03 10 06.69	00 15 49.9	1.36	5.55	0.26	11.1	0.109	18.54	G	PS
J031118+000816	03 11 18.51	00 08 16.4	29.30	36.54	0.81	9.1				PS
J031202−000442	03 12 02.50	−00 04 42.5	6.42	8.59	0.77	5.2	0.038	13.50	G	PS
J031345−000720	03 13 45.04	−00 07 20.3	3.63	6.06	0.62	6.1	2.519	20.04	Q	PS
J031353−000004	03 13 53.47	−00 00 04.1	10.13	7.03	1.47	7.7		21.16	G	PS
J031357+003506	03 13 57.10	00 35 06.9	16.54	20.23	0.83	6.7				PS
J031452+001346	03 14 52.08	00 13 46.5	6.77	10.05	0.69	7.3	3.202	19.54	Q	PS
J031609+000107	03 16 09.55	00 01 07.9	4.02	6.03	0.69	4.6				PS
J031634−002039	03 16 34.96	−00 20 39.6	18.17	15.63	1.18	5.5				PS
J031814−002948[f]	03 18 14.43	−00 29 48.9	113.20	93.91	1.22	9.7		21.77	G	PS
J032007+000354	03 20 07.01	00 03 54.0	12.17	10.20	1.22	5.0		22.10	G	PS
J212000−001159	21 20 00.72	−00 11 59.5	42.94	48.33	0.90	4.9				PS
J212447+000747	21 24 47.34	00 07 47.6	5.79	3.82	1.56	5.3				PS
J213206+003520	21 32 06.15	00 35 20.1	13.65	11.95	1.16	4.1				PS
J213638+004154[f]	21 36 38.57	00 41 54.3	4136.68	3546.71	1.18	8.3	1.932[e]	16.79	q	PS
J213748+001219	21 37 48.43	00 12 19.9	41.69	36.02	1.17	7.0	1.666[e]	17.92	q	PS
J213804+000714	21 38 04.06	00 07 14.7	10.31	16.33	0.64	11.6				CJ
J214138+000319	21 41 38.55	00 03 19.8	11.08	14.37	0.79	6.8				PS
J214324+003502	21 43 24.37	00 35 02.7	36.03	45.22	0.81	9.7	2.030[e]	19.37	q	PS
J214419+002055	21 44 19.88	00 20 55.8	10.34	7.31	1.44	7.5				PS
J214613+000930	21 46 13.31	00 09 30.8	9.94	7.88	1.29	5.6				PS
J214807−000630	21 48 07.73	−00 06 30.6	68.57	90.18	0.77	12.7				CJ
J214811−001230	21 48 11.48	−00 12 30.6	7.76	9.95	0.80	4.7				CJ
J215349+003119	21 53 49.75	00 31 19.6	82.50	103.65	0.81	10.4				PS
J215353−001339	21 53 53.89	−00 13 39.5	13.48	17.27	0.79	7.3				PS
J215359+004412	21 53 59.83	00 44 12.6	9.76	6.73	1.48	7.8	1.030[e]	19.07	q	PS
J215733−000340[f]	21 57 33.66	−00 03 40.5	5.36	3.60	1.53	4.9				PS
J215949+005146	21 59 49.91	00 51 46.7	12.29	9.21	1.36	7.8				PS
J215954−002150	21 59 54.46	−00 21 50.1	4.07	2.46	1.71	4.7	1.960[e]	16.98	q	PS
J220017−000133	22 00 17.37	−00 01 33.6	7.84	6.15	1.30	4.9				CL
J220755−000215	22 07 55.25	−00 02 15.0	78.40	61.93	1.28	11.9				CJ
J220822+002352	22 08 22.88	00 23 52.7	4.62	2.42	1.97	6.1				PS
J221001−001309[f]	22 10 01.82	−00 13 09.9	125.83	115.31	1.10	4.8				PS
J221031−001356	22 10 31.46	−00 13 56.1	14.06	12.00	1.19	5.2				PS
J221909+003113	22 19 09.40	00 31 13.4	9.13	11.70	0.80	5.3				CJ

TABLE 2—*Continued*

Source / Component	RA (J2000) (core component)	Dec (J2000)	F_{2002} [mJy]	F_{1995} [mJy]	FR[a]	S[b]	z[c]	r[c]	ID[c]	RM[d]
J222036+003334	22 20 36.33	00 33 34.2	15.27	12.76	1.22	5.8				PS
J222135−001100	22 21 35.00	−00 11 00.1	14.11	8.64	1.66	12.6				PS
J222235+001536	22 22 35.87	00 15 36.7	46.04	51.13	0.91	4.5				CJ
J222704+004517	22 27 04.24	00 45 17.5	8.13	5.57	1.49	7.0				PS
J222726+001059	22 27 26.53	00 10 59.3	6.05	4.52	1.37	4.2				PS
J222729+000522	22 27 29.08	00 05 22.2	77.84	91.64	0.86	7.4	1.510[e]	18.86	q	CL
J222744+003450	22 27 44.58	00 34 50.6	22.13	30.53	0.74	12.1	1.540[e]	19.14	q	PS
J222758+003705	22 27 58.13	00 37 05.2	68.69	99.12	0.70	17.3				PS
J223047+002756	22 30 47.46	00 27 56.3	8.54	13.82	0.63	11.4				PS
J224224+005512	22 42 24.14	00 55 13.0	17.71	13.44	1.34	9.5				CJ
J224331−001233	22 43 31.94	−00 12 33.1	13.85	21.40	0.66	14.8	2.040[e]	18.45	q	PS
J224448−000619	22 44 48.11	−00 06 19.8	8.24	5.58	1.51	7.3				PS
J224627−001214[f]	22 46 27.68	−00 12 14.2	85.55	56.00	1.55	20.9				PS
J224730+000006[f]	22 47 30.19	00 00 06.1	464.52	183.71	2.56	43.8	0.094[e]	18.50	q	PS
J224922+001804	22 49 22.28	00 18 04.6	10.41	8.51	1.25	5.3				PS
J225852−001857	22 58 52.94	−00 18 57.3	3.45	1.28	2.80	6.0				PS
J230157+000351	23 01 57.85	00 03 52.0	3.75	7.04	0.55	7.8		23.23	Q	PS
J230314+000052	23 03 14.85	00 00 52.2	3.72	1.72	2.24	5.8				PS
J230655+003638	23 06 55.16	00 36 38.1	12.99	15.19	0.87	4.3				PS
J231541+002936	23 15 41.67	00 29 36.6	21.93	13.94	1.60	15.7		20.81	Q	PS
J231558−001205	23 15 58.64	−00 12 05.5	3.52	6.27	0.58	7.0		22.85	G	PS
J231845−000754	23 18 45.81	−00 07 54.7	3.03	5.34	0.59	5.5	0.867	19.44	Q	PS
J231856+001437[g]	23 18 56.66	00 14 37.7	20.16	18.34	1.12	4.2	0.030	12.76	G	PS
J231910+001859	23 19 10.33	00 18 59.0	28.90	33.36	0.88	5.6		22.60	Q	PS
J232038+003139	23 20 38.01	00 31 39.8	72.69	82.95	0.89	5.7	1.911	19.03	Q	PS
J232323+003327	23 23 23.95	00 33 27.5	16.73	12.52	1.36	9.2				PS
J233448−001400	23 34 48.06	−00 14 01.0	24.85	29.64	0.85	6.8		21.56	Q	PS
J233822+001146	23 38 22.35	00 11 46.6	18.19	15.44	1.20	6.0		22.24	Q	PS
J233852+004843	23 38 52.46	00 48 43.5	11.32	9.18	1.26	5.9				PS
J234623+004301	23 46 23.73	00 43 01.1	13.49	11.79	1.17	4.6	2.861	19.09	Q	PS
J234939−001315	23 49 39.90	−00 13 15.2	8.46	6.97	1.24	4.2	1.267	20.22	Q	PS
J235022+001232	23 50 22.41	00 12 32.4	3.92	2.03	2.00	5.1				PS
J235050−002848	23 50 50.72	−00 28 48.7	13.12	11.57	1.15	4.1		19.62	G	CL
J235409−001948[f]	23 54 09.18	−00 19 48.1	384.58	344.79	1.13	6.1	0.462	17.93	Q	PS
J235823+000213	23 58 23.91	00 02 13.2	8.03	10.67	0.77	5.7				PS
J001800+000313[h]	00 18 00.79	00 03 17.9	20.76	18.82	1.12	4.2				HS
J003246−001917[h]	00 32 46.02	−00 19 17.8	81.29	60.80	1.35	14.5				HS
J212058+000612[h]	21 20 59.00	00 06 12.7	31.17	28.05	1.13	5.3				HS
J212955+000758[h]	21 29 55.68	00 07 59.0	1.17	3.03	0.42	4.5				CL
J235828+003934[h]	23 58 28.77	00 39 34.1	2.48	4.16	0.62	4.3				CL

[a]Corrected flux density ratio, see Eqn. 5.

[b]Significance (in units of σ rms) as defined by: $S = \left| \frac{\mathrm{FR}_{-1}}{\chi(\mathrm{FR}_{+1})} \right|$, using the χ definition from Eqn. 4.

[c]SDSS redshift, r-band magnitude, and optical identification, except where noted. Sources in the list with RA

between 21^h and 23^h are not covered by SDSS DR1.

[a]Radio morphology: PS=pointsource, CJ=core-jet, CL=core + lobes, CX=complex, CH=core + halo, and HS=possible hotspot.

[e]Redshift taken from literature. If the ID is in lower case then the optical data are from the literature as well.

[f]Also meets the FZDB-NVSS variability criterion. Only sources brighter in the FZDB epoch were considered.

[g]NGC 7603

[h]Variability of this source is spurious (see Sect. 4)

TABLE 3
APM MATCH STATISTICS, 3″ SEARCH RADIUS

Sample[a]	Detected	Rate
Variable	66	53.7%
Control 1	17	13.8%
Control 2	29	23.6%
Control 3	21	17.1%
Control 4	21	17.1%
Control 5	20	16.3%
Control 6	27	22.0%
Control 7	23	18.7%
Control 8	17	13.8%
Control 9	21	17.1%
Control 10	22	17.9%
Control 11	23	18.7%
Control 12	21	17.1%
Mean Control	21.8±3.5	17.7±2.8%

[a]All samples contain 123 sources

TABLE 4
SDSS MATCH STATISTICS, 3″ SEARCH RADIUS

Sample[a]	Detected	Rate	Quasars[b]	Galaxies[b]
Variable	64	82.0%	53.1%	46.9%
Control 1	28	37.3%	17.9%	82.1%
Control 2	30	40.0%	13.3%	86.7%
Control 3	21	28.0%	14.3%	85.7%
Control 4	36	48.0%	13.9%	86.1%
Control 5	26	34.7%	26.9%	73.1%
Control 6	32	42.7%	18.8%	81.2%
Control 7	29	38.7%	24.1%	75.9%
Control 8	33	44.0%	9.1%	90.9%
Control 9	23	30.7%	21.7%	78.3%
Control 10	30	40.0%	16.7%	83.3%
Control 11	31	41.3%	29.0%	71.0%
Control 12	22	29.3%	18.2%	81.8%
Mean Control	28.4±4.6	37.9±6.2%	18.7±5.9%	81.3±5.9%

[a]Only 75 out of 123 variable sources are covered by the SDSS DR1 data. The rates have been corrected accordingly.

[b]Relative fraction of quasars and galaxies, based on the SDSS morphology.

TABLE 5
MEAN OPTICAL COLORS OF VARIABLE AND NON-VARIABLE SAMPLES

Sample	(U-R)	(R-Z)
Quasars - variable	0.89±0.13	0.40±0.07
non-variable	1.37±0.17	0.60±0.08
nominal offset[a]	−0.48	−0.20
significance[b]	2.3	1.8
Galaxies - variable	1.81±0.21	1.09±0.11
non-variable	2.28±0.09	1.20±0.05
nominal offset[a]	−0.47	−0.11
significance[b]	2.0	0.9

[a]Between non-variable and variable samples.

[b]Defined as nominal offset divided by the rms of the uncertainties.